Mon. Not. R. Astron. Soc. **000**, ??–?? (2014) Printed 16 September 2014 (MN LATEX style file v2.2)

The extinction law inside the 30 Doradus nebula⋆

Guido De Marchi[1] and Nino Panagia,[2,3,4]
[1]*European Space Research and Technology Centre, Keplerlaan 1, 2200 AG Noordwijk, The Netherlands, gdemarchi@esa.int*
[2]*Space Telescope Science Institute, 3700 San Martin Drive, Baltimore, MD 21218, USA, panagia@stsci.edu*
[3]*INAF–NA, Osservatorio Astronomico di Capodimonte, Salita Moiariello 16, 80131 Naples, Italy*
[4]*Supernova Ltd, OYV #131, Northsound Rd., Virgin Gorda VG1150, Virgin Islands, UK*

arXiv:1408.4786v4 [astro-ph.SR] 15 Sep 2014

Received 13 May 2014; Accepted 18 August 2014

ABSTRACT

We have studied the interstellar extinction in a field of $\sim 3' \times 3'$ at the core of the 30 Doradus nebula, including the central R 136 cluster, in the Large Magellanic Cloud. Observations at optical and near-infrared wavelengths, obtained with the WFC 3 camera on board the *Hubble Space Telescope*, show that the stars belonging to the red giant clump are spread across the colour–magnitude diagrams because of the considerable and uneven levels of extinction in this region. Since these stars share very similar physical properties and are all at the same distance, they allow us to derive the absolute extinction in a straightforward and reliable way. Thus we have measured the extinction towards about 180 objects and the extinction law in the range $0.3 - 1.6\,\mu$m. At optical wavelengths, the extinction curve is almost parallel to that of the diffuse Galactic interstellar medium. Taking the latter as a template, the value of $R_V = 4.5 \pm 0.2$ that we measure indicates that in the optical there is an extra grey component due to a larger fraction of large grains. At wavelengths longer than $\sim 1\,\mu$m, the contribution of this additional component tapers off as $\lambda^{-1.5}$, like in the Milky Way, suggesting that the nature of the grains is otherwise similar to those in our Galaxy, but with a ~ 2.2 times higher fraction of large grains. These results are consistent with the addition of "fresh" large grains by supernova explosions, as recently revealed by *Herschel* and *ALMA* observations of SN 1987A.

Key words: Hertzsprung–Russell and colour–magnitude diagrams — dust, extinction — Magellanic Clouds

1 INTRODUCTION

Studies of the properties of stellar populations hinge on the accurate knowledge of the amount and properties of interstellar extinction, since they affect fundamental observational quantities such as the distance and luminosity function (e.g. Gottlieb & Upson 1969). The diffuse Galactic interstellar medium (ISM) appears to have a rather uniform extinction law and the ratio of total and selective extinction $R_V = A_V/E(B-V)$ is found to be consistently about 3.1 (e.g. Savage & Mathis 1979). However, in star forming regions the situation is rather different: R_V varies considerably in our Galaxy and studies conducted over the past 40 years have revealed a wide variety of extinction curves (e.g. Bless & Savage 1972; Seaton 1979; Fitzpatrick 1998, 1999). In particular, in dense star forming regions the situation is quite different from that of the diffuse ISM and generally the value of R_V appears to increase (e.g. Johnson & Mendoza 1964; Savage & Mathis 1979; Cardelli, Clayton & Mathis 1988), due to the presence of larger grains, with a correspondingly rather different shape of the extinction curve.

Nonetheless, there appears to be some commonality in the properties of the extinction in these environments. Even though the extinction curves are effectively different, Cardelli, Clayton & Mathis (1989) have shown that the properties of the extinction at optical and near-infrared (NIR) wavelengths appear to be correlated with those in the ultraviolet, and the measured $A(\lambda)/A(V)$ can generally be described by one family of curves depending only on R_V. For instance, Valencic, Clayton & Gordon (2004) compiled a homogeneous database of 417 extinction curves towards Galactic stars, finding that 93 % of them are compatible with the R_V-dependent extinction parameterization of Cardelli et al. (1989), within the uncertainties. Fitzpatrick & Massa (2007) offer a different interpretation of the results by Valencic et al. (2004), pointing out that the dependence of $A(\lambda)/A(V)$ on R_V only is partially caused by the fact that $A(\lambda)/A(V)$ is derived from the measured colour excess by taking the value of R_V into account, therefore necessarily causing some degree of apparent correlation. According to Fitzpatrick & Massa (2007), extinction curves are not a one-parameter family in R_V and a variety of curves remains even in our Galaxy.

⋆ Based on observations with the NASA/ESA *Hubble Space Telescope*, obtained at the Space Telescope Science Institute, which is operated by AURA, Inc., under NASA contract NAS5-26555.

© 2014 RAS

In this work we do not address the matter of the functional form of the extinction laws, but rather concentrate on the physical properties of the extinction inside the Tarantula nebula (30 Dor). A robust determination of the extinction curve in this environment is crucial for modern Astronomy, since this object is the closest and only known starburst in the Local Group. The strength of star formation in 30 Dor and the number of massive stars that it harbours are similar to those found in interacting galaxies in the local Universe and in young galaxies at high redshift ($z > 5$, e.g. Meurer et al. 1997; Shapley et al. 2003; Heckman et al. 2004). Furthermore, with a metallicity of the order of 1/3 $Z_\odot$ (e.g. Hill, Andrievsky & Spite 1995; Geha et al. 1998), 30 Dor allows us to probe the prevailing conditions at redshift $z \gtrsim 2$, when star formation was at its peak in the Universe (e.g. Madau et al. 1996; Lilly et al 1996). Thus, determining the properties of the extinction in 30 Dor will not only allow us to understand how star formation is proceeding in this specific Large Magellanic Cloud (LMC) environment, but also in a cosmological sense.

Gordon et al. (2003) have carried out an exhaustive study of the extinction properties in the LMC towards 19 different lines of sight, extending previous investigations by Clayton & Martin (1985) and Misselt, Clayton & Gordon al. (1999). They find that only four of the 19 sight lines probed appear to be compatible with the R_V-dependent family of extinction curves of Cardelli et al. (1989), thereby revealing a wider variety than in the Milky Way. Unfortunately, none of the sight lines probe specifically the 30 Dor region: although 8 of them are associated with the LMC2 Supershell near the Tarantula nebula, the nearest star is $\sim 9'$ away from the centre of 30 Dor and the others are beyond $15'$, with a median distance of $\sim 20'$, typically probing a projected distance of ~ 300 pc or three times the radius of the nebula (Lebouteiller et al. 2008).

Until recently, the most accurate empirical determination of the extinction law inside 30 Dor was the 30-year old study by Fitzpatrick & Savage (1984). These authors used the traditional approach of the "pair method," in which the flux distribution or colours of a reddened object are compared with those of a reference star of the same spectral type (*e.g.,* Johnson 1968; Massa, Savage & Fitzpatrick 1983; Cardelli, Sembach & Mathis 1992). This method is very reliable and can detect subtle variations of the extinction law with the environment, but it works optimally if using targets such as massive stars with high quality spectra extending from the near ultraviolet to the NIR.

Given the level of crowding present inside 30 Dor, the extinction law derived by Fitzpatrick & Savage (1984) is based on just a handful of lines of sight (namely 7 within the central $5'$ of R 136a). This situation has been recently improved by Maíz Apellániz et al. (2014), who used a Bayesian approach to derive the so-called "extinction without standards" (Fitzpatrick & Massa 2005) at optical and some NIR wavelengths towards 83 OB stars in the inner $2'$ radius of R 136. This work indicates that the extinction is variable in the field and R_V is typically in the range $4 - 5$. On the other hand, these early-type massive stars do not necessarily sample the same environment in which low-mass stars form (e.g. De Marchi, Panagia & Sabbi 2011), and due to their short life they cannot reveal the long-term evolution of the dust grains in those regions. In other words, massive stars only allow us to probe the most active star-forming environments at the peak of the burst, but those conditions are not characteristic of all objects in the field.

To overcome these limitations, we have developed a new method to unambiguously determine the absolute value of the extinction in a uniform way across a field such as that of 30 Dor (De Marchi, Panagia & Girardi 2014; hereafter Paper I). Our method makes use of multi-band photometry of red giant stars belonging to the red clump (RC). Other authors have used RC observations in the past to study the reddening distribution and to derive reddening maps in the LMC (e.g. Zaritsky 1999; Haschke et al. 2011; Tatton et al. 2013). However, all these works have assumed an extinction law and therefore cannot derive it independently.

Applied to a typical field in the Magellanic Clouds, such as 30 Dor, our method offers many advantages: *(i)* all RC stars on which we operate are at the same distance, to better than 1 %; *(ii)* they have very similar intrinsic physical properties in all bands, within 0.05 mag for similar age and metallicity; *(iii)* our statistics is very solid, with about 20 stars arcmin^{-2} or ~ 150 objects in a typical *Hubble Space Telescope* (HST) pointing; and *(iv)* we derive a self-consistent absolute extinction curve over the entire wavelength range covered by the photometry with no need for spectroscopic observations. This method can be easily extended to other nearby galaxies.

In this work, we apply our method to the panchromatic observations of 30 Dor in the range $0.3 - 1.6\,\mu$m collected in 2009 with the WFC 3 instrument on board the HST (De Marchi et al. 2011a). The structure of the paper is as follows. The observations are presented in Section 2, while the selection of RC stars is discussed in Section 3. Section 4 is devoted to deriving the absolute extinction towards RC stars and the corresponding extinction law. In Section 5 we discuss the reddening distribution in this field. A summary and our conclusions follow in Section 6.

Table 1. Number of exposures and cumulative exposure times in the various bands.

Filter	Band	$N_{\rm exp}$	$t_{\rm tot}$
F336W	(U)	24	8 659 s
F438W	(B)	16	5 174 s
F555W	(V)	20	6 892 s
F656N	($H\alpha$)	8	10 805 s
F814W	(I)	20	10 700 s
F110W	(J)	9	1 518 s
F160W	(H)	12	7 816 s

2 OBSERVATIONS AND DATA ANALYSIS

The observations used in this work were obtained in 2009 October using the WFC 3 camera on board the HST, and are extensively described in De Marchi et al. (2011a). The filters used, the number of exposures and their total durations are listed in Table 1. The observations made use of an extensive dithering pattern, combining long and short exposures, in order to improve the sampling of the telescope's point spread function and increase the dynamic range of the photometry.

Figure 1 shows a region of about $2'\times2'$ at the centre of the field covered by the observations (the total area covered spans $2\farcm7\times2\farcm7$). The bright cluster in the field is R 136. The panel on the left provides a colour-composite, with the blue channel obtained by averaging the F336W and F439W filters, the F555W filter serves as green channel, the F814W filter as red channel and the F656N filter is used as orange. The panel on the right results from the combination of the F110W and F160W filters, assigned respectively to complementary teal and orange colours.

Also the photometry is extensively discussed in De Marchi et

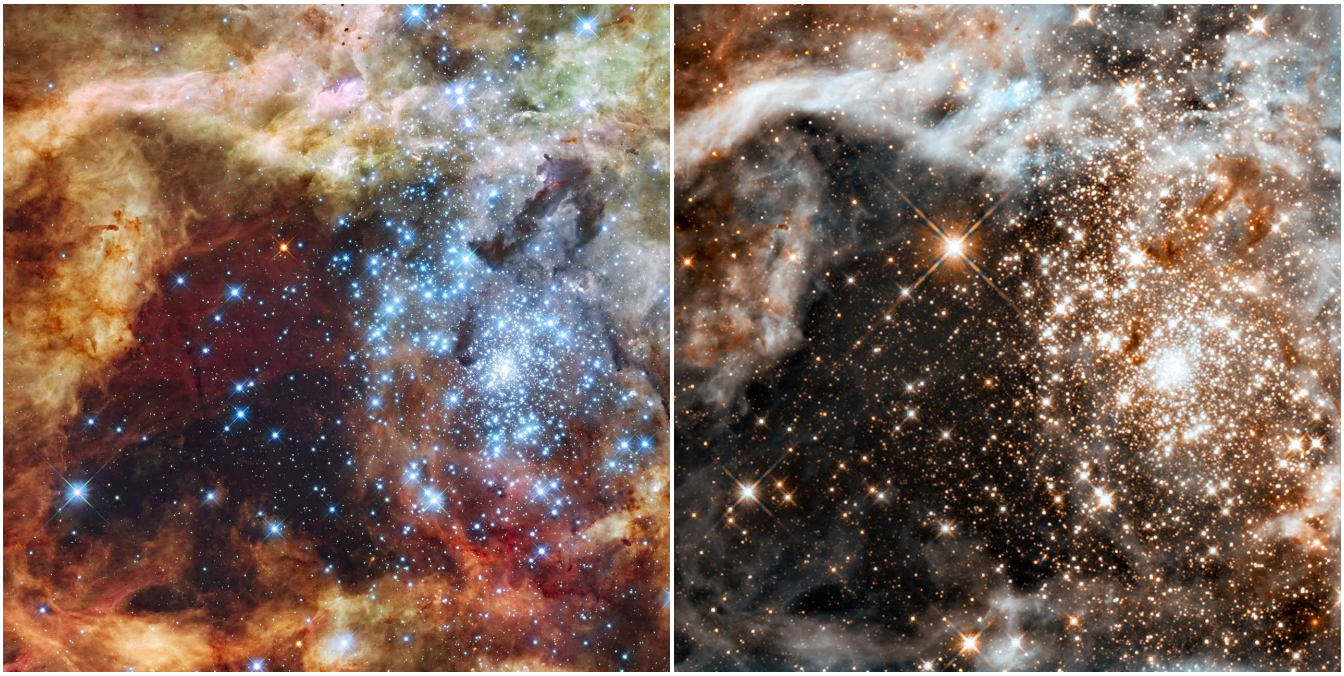

Figure 1. Optical (left) and NIR (right) colour-composite images of a region of $\sim 2' \times 2'$ at the centre of the field covered by the observations. In the left panel the colours are as follows: the blue channel is the average of F336W and F438W, the green channel is F555W, the red channel F814W, and orange is provided by F656N. In the right panel, the F110W and F160W filters are assigned respectively to complementary teal and orange. North is inclined 14 deg to the left of the vertical and east is to its left. (These images were released by the Space Telescope Science Institute on 2009 December 15 as part of News Release number STScI-2009-32.)

al. (2011a), to whom we refer the reader for further details. As an example, we show in Figure 2 the I *vs* $B-V$ colour–magnitude diagram (CMD), compared with the zero age main sequence (ZAMS) from the models of Marigo et al. (2008; thin dashed line, extending up to 60 $M_\odot$) for the specific WFC 3 filters used here and a metallicity of $Z = 0.007$ as appropriate for R 136 and the young LMC population in general (e.g. Hill, Andrievsky & Spite 1995; Geha et al. 1998). As for the distance modulus, we have assumed $(m - M)_0 = 18.6$ (Panagia et al. 1991; Panagia 1999; Walborn & Blades 1997). Only objects with combined photometric uncertainty in the four optical broad bands smaller than 0.1 mag are shown in Figure 2. The combined photometric uncertainty δ_4 is defined by Romaniello (1998) as:

$$\delta_4 = \sqrt{\frac{\delta_{336}^2 + \delta_{438}^2 + \delta_{555}^2 + \delta_{814}^2}{4}} \qquad (1)$$

where δ_{336}, δ_{438}, δ_{555}, and δ_{814} are the uncertainties in each individual band.[1] The ZAMS is also already reddened by the amount corresponding to the foreground Milky Way (MW) absorption along the line of sight, which Fitzpatrick & Savage (1984) estimated to be $E(B-V) = 0.07$ or $A_V = 0.22$. The comparison shows that there is an additional extinction component in front of 30 Dor, intrinsic to the LMC, which is known for a long time (e.g. Fitzpatrick & Savage 1984). Furthermore, a comparison of the width of the upper main sequence (MS) with the photometric uncertainties quoted above confirms that there is differential reddening in the field, as already reported elsewhere (e.g. Hunter et al. 1995; De Marchi et al. 2011a). The goal of this work is to determine the amount and type of extinction in this field and the corresponding properties of the ISM. As mentioned in the Introduction, to this purpose we will use the RC objects present in the field.

[1] The definition given by Equation 1 can be generalised for any combination of bands. For instance, in Section 5 we will also refer to the combined photometric uncertainty δ_3 in the B (F438W), V (F555W) and I (F814W) bands. For details on the photometric uncertainty in the individual bands, see De Marchi et al. (2011a).

3 RED CLUMP STARS

In order to determine the extinction curve in this field, as discussed by De Marchi, Panagia & Girardi (2014; Paper I), it is necessary to identify the bona-fide RC stars and to measure their displacement in the CMD from the location that they would occupy in the absence of extinction. The procedure has three main steps, namely the identification of the candidate RC stars, the removal of possible outliers, and the determination of the slope of the reddening vector in each set of bands. The steps are carried out separately in each of the eight CMDs built with our set of bands as a function of the $m_{438} - m_{555}$ and $m_{555} - m_{814}$ colours. However, since the NIR observations do not cover the entire field, the primary selection of RC objects is based on the four optical bands.

3.1 Identification of candidate RC stars

We take as starting location the "nominal RC," defined as the theoretical RC of stars of the lowest metallicity consistent with the observations. In Paper I we concluded that the most appropriate metallicity for the old stars (> 1 Gyr) in the field around the 30 Dor region is $Z = 0.004$. This choice defines the magnitude of the nom-

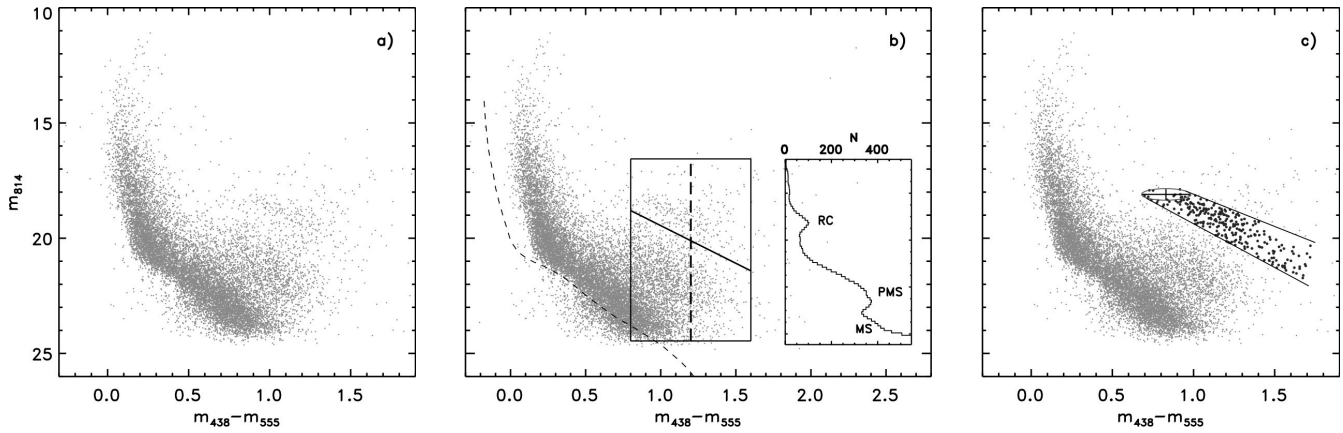

Figure 2. Panel **a)**: As an example, we show the CMD in the *B*, *V*, and *I* bands. Only stars with $\delta_4 < 0.1$ are included (the typical photometric uncertainty is comparable with the size of the dots in the figure). RC stars define a prominent sequence almost parallel to the low-mass MS but well separated from it and from the PMS stars. Panel **b)**: We characterize the separation between RC and MS stars. The apparent slope of the RC sequence is indicated by the tilted solid line in the central box, while the ZAMS is indicated by the thin dashed curve, from the models of Marigo et al. (2008), for the distance to the LMC and already including intervening Galactic extinction. The inset on the right-hand side shows the number of objects contained in slices parallel to the RC sequence as a function of magnitude. The density peaks corresponding to the RC and PMS stars are distinct and clearly visible. Panel **b)**: the initial selection of candidate RC stars includes all objects with $\delta_4 < 0.1$ located inside the theoretical RC error ellipse or contained between the two tangents to it. The slope of the tangents is that of the approximate reddening vector with an added 15 % uncertainty. Candidate RC stars are identified in the same way in all CMDs.

Table 2. Apparent magnitudes $m_{\rm RC}$ of the RC and corresponding 1 σ spread in all bands, already including the effects of the intervening MW extinction.

Filter	Band	$m_{\rm RC}$	σ
F336W	(*U*)	20.34	0.12
F438W	(*B*)	19.98	0.10
F555W	(*V*)	19.16	0.08
F814W	(*I*)	18.10	0.08
F110W	(*J*)	17.72	0.10
F160W	(*H*)	17.15	0.10

inal RC, whereas for the colour we take the average RC colours of stars in the range 1.4 – 3.0 Gyr, as in Paper I.

The corresponding apparent magnitudes and associated 1 σ spread are shown in Table 2, while the colours in the most common band combinations are $m_{438} - m_{555} = 0.83 \pm 0.06$, $m_{555} - m_{814} = 1.06 \pm 0.04$. These magnitudes already include the effects of the foreground MW extinction, *i.e.* $E(B-V) = 0.07$ or $A_V = 0.22$ as mentioned above (Fitzpatrick & Savage 1984).

An inspection of the CMDs (see as an example Figure 2a) immediately reveals the candidate RC objects, as they define a prominent sequence almost parallel to the MS but well separated from it and from the pre-main sequence (PMS) stars.

To confirm that the candidate RC stars are distinct from the MS objects, we characterize their separation in a quantitative way, by calculating the number of stars inside slanted slices, parallel to one another and progressively fainter. The slope of the slices is that defined by the apparent slope of the extinguished RC sequence in the CMD and it is shown by the tilted solid line in Figure 2b. In this example the slices are 0.1 mag thick and are contained within the box shown at the centre of the figure. The total number of objects in each slice is shown by the histogram in the inset at the right-hand side of Figure 2b, as a function of the magnitude. The vertical scale is shifted in such a way that the peaks in the histogram are shown at the magnitudes that correspond to the intersection of the reddening vector (tilted solid line) with the median of the box (vertical dashed line). The density peaks corresponding to the RC and PMS stars are distinct and clearly visible, and so is the sharply increasing ramp due to MS stars.

The actual selection of candidate RC stars is done separately in each CMD, i.e. those obtained by plotting the magnitudes in all bands as a function of $m_{438}-m_{555}$ and $m_{555}-m_{814}$. After determining the approximate direction of the reddening vector (see the tilted solid line in Figure 2b for the specific CMD shown there), we plot the location of the theoretical RC and trace two lines tangent the error ellipse defined by 2.5 σ. The slope of the tangents is that of the approximate reddening vector with an added 15 % uncertainty. This is done separately for each CMD and as an example we show in Figure 2c the case of the CMD in the m_{814} *vs.* $m_{438} - m_{555}$ bands (corresponding to *I vs.* $B - V$). In each CMD se take as candidate RC stars those inside the region defined by the error ellipse and its tangents. These objects are marked as thicker dots in Figure 2b.

We repeat this procedure in the CMDs resulting from all combinations of bands as a function of the $m_{438} - m_{555}$ and $m_{555} - m_{814}$ colours, since those exist for all objects in the field, deriving in this way eight sets of candidate RC objects. In the most conservative approach, we retain as bona-fide RC stars only the objects that satisfy this condition simultaneously in all optical bands, *i.e.,* a total of 146 stars. We cannot impose the same conditions for stars observed through the NIR bands, since those observations cover a more limited area than the optical bands. Therefore, we take as candidate RC objects in those bands all those that are present in the photometry and are classified as RC stars in all other bands simultaneously. In total there are 93 such objects.

3.2 Removal of possible outliers

In order to guarantee that our RC candidate stars have physical properties consistent with those of this class of objects, we have further excluded from this sample a total of 6 stars that have Hα equivalent width $W_{\rm eq}(H\alpha) > 3$ Å, as they could be PMS stars (three

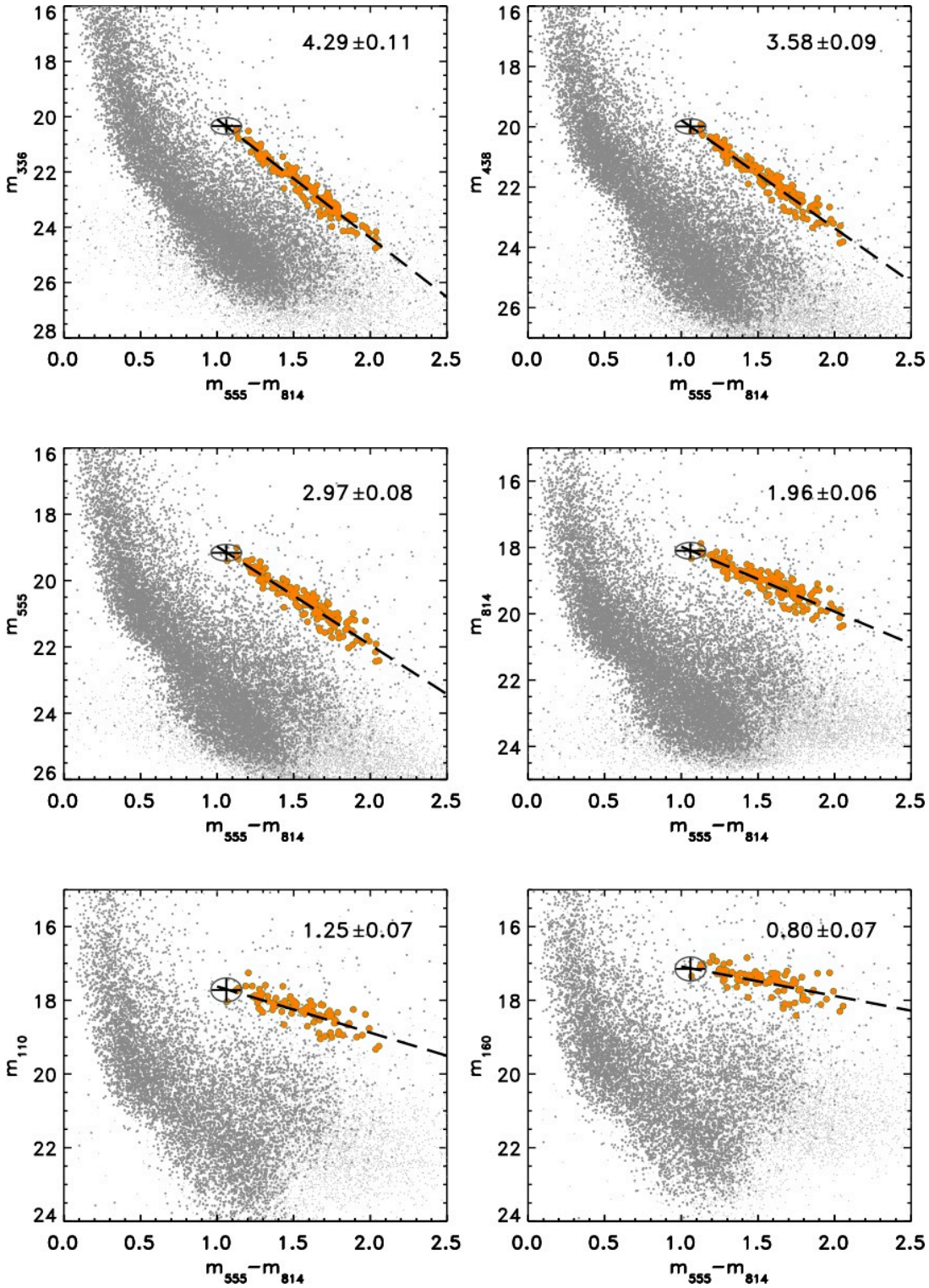

Figure 3. CMDs as a function of the $m_{555} - m_{814}$ colour. The thick orange dots are the the 140 bona-fide RC stars (90 of which are also are visible in the NIR bands). The nominal location of the RC is shown by the ellipses in each graph and the best-fitting reddening vectors are indicated by the dashed lines. The value of the parameter R and its uncertainty are given in each panel.

of them also fall in the area covered by the NIR observations). Objects with Hα excess emission are easily identified following the method described by De Marchi, Panagia & Romaniello (2010) and De Marchi et al. (2010b), to which we refer the reader for more details.

As shown in De Marchi et al. (2011a), there is a large population of PMS stars in this field and some of them have colours and magnitudes that place them in the CMD region occupied by extinguished RC objects. It is well known that also chromospheric activity is a likely source of Hα emission in stars of low mass such

Table 3. Measured values of the ratio R between absolute (A) and selective (E) extinction in the specific bands of our observations, with corresponding uncertainties. The effective wavelength (λ) and wave number ($1/\lambda$) of each band are also indicated.

Band combination	R	λ [Å]	$1/\lambda$ [μm^{-1}]
$A_{336}/E(m_{438}-m_{555})$	6.81 ± 0.34	3 359	2.98
$A_{438}/E(m_{438}-m_{555})$	5.73 ± 0.29	4 332	2.31
$A_{555}/E(m_{438}-m_{555})$	4.79 ± 0.25	5 339	1.87
$A_{814}/E(m_{438}-m_{555})$	3.24 ± 0.18	8 060	1.24
$A_{110}/E(m_{438}-m_{555})$	2.20 ± 0.18	11 608	0.86
$A_{160}/E(m_{438}-m_{555})$	1.52 ± 0.16	15 387	0.65
$A_{336}/E(m_{555}-m_{814})$	4.29 ± 0.11	3 359	2.98
$A_{438}/E(m_{555}-m_{814})$	3.58 ± 0.09	4 332	2.31
$A_{555}/E(m_{555}-m_{814})$	2.97 ± 0.08	5 339	1.87
$A_{814}/E(m_{555}-m_{814})$	1.96 ± 0.06	8 060	1.24
$A_{110}/E(m_{555}-m_{814})$	1.25 ± 0.07	11 608	0.86
$A_{160}/E(m_{555}-m_{814})$	0.80 ± 0.07	15 387	0.65

as those in the RC phase. However, as discussed in Paper I, White & Basri (2003) indicate specific thresholds above which stars with Hα excess emission should be considered classical T Tauri stars, instead of just chromospherically active objects.

For stars of spectral type K0 – K5, White & Basri (2003) recommend thresholds of 3 Å, and values larger than 10 Å for K7 – M2.5 stars. Since these interlopers, like the RC stars, are affected by reddening, we cannot determine their actual spectral type. Thus, we make the most conservative assumption that they are all of spectral type earlier than K0 and exclude from the bona-fide sample of RC stars a total of 6 sources that have $W_{\rm eq}(H\alpha) > 3$ Å, of which 3 also fall in the area covered by the NIR observations. The final count of bona-fide RC stars includes 140 objects detected in all optical bands, of which 90 have also been measured through the NIR filters. The bona-fide RC stars are shown as thick orange dots in the CMDs of Figure 3.

3.3 Deriving the slope of the reddening vectors

As discussed in Paper I, in each CMD we derive the best linear fit to the distribution of the bona-fide objects taking into account: *1)* the uncertainties on their magnitudes and colours; *2)* the uncertainties on the ellipse defining the model RC in each individual CMD; *3)* an equal number (140 or 90 depending on the bands) of synthetic un-reddened RC stars with a Gaussian distribution inside the ellipses. The latter step guarantees that the best linear fit passes through the centre of the nominal RC. The reddening slopes derived in this way correspond to the value of the ratio R between absolute and selective extinction in the specific bands of our observations. The values of the ratio R and the corresponding uncertainties are listed in Table 3. The reddening slopes are also shown by the thick dashed line in the CMDs of Figure 3, where all stars in our photometric catalogue are shown. The thick orange dots are the bona-fide RC stars, while the light- and dark-grey smaller dots are for stars with, respectively, δ_4 photometric uncertainty larger or smaller than 0.1 mag. The values of R are also indicated in each panel.

4 EXTINCTION LAW

It is customary to express the extinction law in the form of the ratio

$$R_\lambda \equiv \frac{A_\lambda}{E(B-V)}, \qquad (2)$$

where A_λ is the extinction in the specific band and $E(B-V)$ the colour excess in the canonical Johnson B and V bands. The values of R_λ listed in Table 3 do not exactly correspond to Equation 2, since the colour excess is the one measured in the specific WFC 3 bands used in making these observations. However, we can easily derive the values of R_λ through spline interpolation, as described in Paper I, and can translate in this way the values of Table 3 into the corresponding values as a function of $E(B-V)$ in the traditional Johnson bands.

The R_λ values obtained in this way are shown graphically in Figure 4, where squares and triangles correspond to values obtained originally from measurements as a function of the colour indices $m_{438}-m_{555}$ and $m_{555}-m_{814}$, respectively. The two sets of values are in excellent agreement with one other within their uncertainties. The thick solid line shows a spline interpolation through the R_λ values and takes into account the smaller uncertainties in $m_{555}-m_{814}$. The interpolated R_λ values in the classical Johnson–Cousin bands, at the wavelengths marked by the vertical dotted lines in the figure, are listed in Table 4 (note that the value for the K band is actually an extrapolation and, therefore, is indicated in italics in the table). For comparison, in Figure 4 we also show the R_λ values from Paper I, measured in a field $\sim 6'$ SW of R 136, and the corresponding spline interpolation (long-dashed line), as well as the canonical Galactic extinction law, taken from the work of Fitzpatrick & Massa (1990) for $R_V = 3.1$ (short dashed line).

4.1 Comparison with previous works

The shape of the extinction curve that we obtain is not reproduced by the traditional parameterizations based on the value R_V (*e.g.,* Cardelli et al. 1989; Fitzpatrick & Massa 1990) because they are unable to reproduce the entire wavelength range covered by our observations with a single value of the parameter R_V.

As an example, we show in Figure 4 with a thin grey line the extinction law recently derived for this specific field by Maíz Apellániz et al. (2014). These authors have used spectroscopy and NIR photometry from the VLT-FLAMES Tarantula Survey (Evans et al. 2011) and the same HST optical photometry discussed in this work (De Marchi et al. 2011a) for a selected sample of 83 stars of spectral types O and B (see Section 5). Using the Bayesian code CHORIZOS (Maíz Apellániz 2004), they have fitted the available photometry to a family of synthetic spectral energy distributions, with different assumptions on the stellar parameters and the shape of the extinction law. They conclude that the best family of extinction laws is a slightly modified version of that of Cardelli et al. (1989), since the latter does not provide a good fit to the observations in the U band when R_V is large. At longer optical wavelengths this new family of extinction laws does not deviate from Cardelli et al.'s and Maíz Apellániz et al. (2014) assumed it to be exactly that in the NIR.

Nor are our observations compatible with the extinction curve derived by Gordon et al. (2003) from 8 sight lines around 30 Dor. As mentioned in the Introduction, these stars are outside the clusters at a median distance of $\sim 20'$ from its centre. The extinction curve of Gordon et al. (2003) is shown as a triple-dot-dashed line

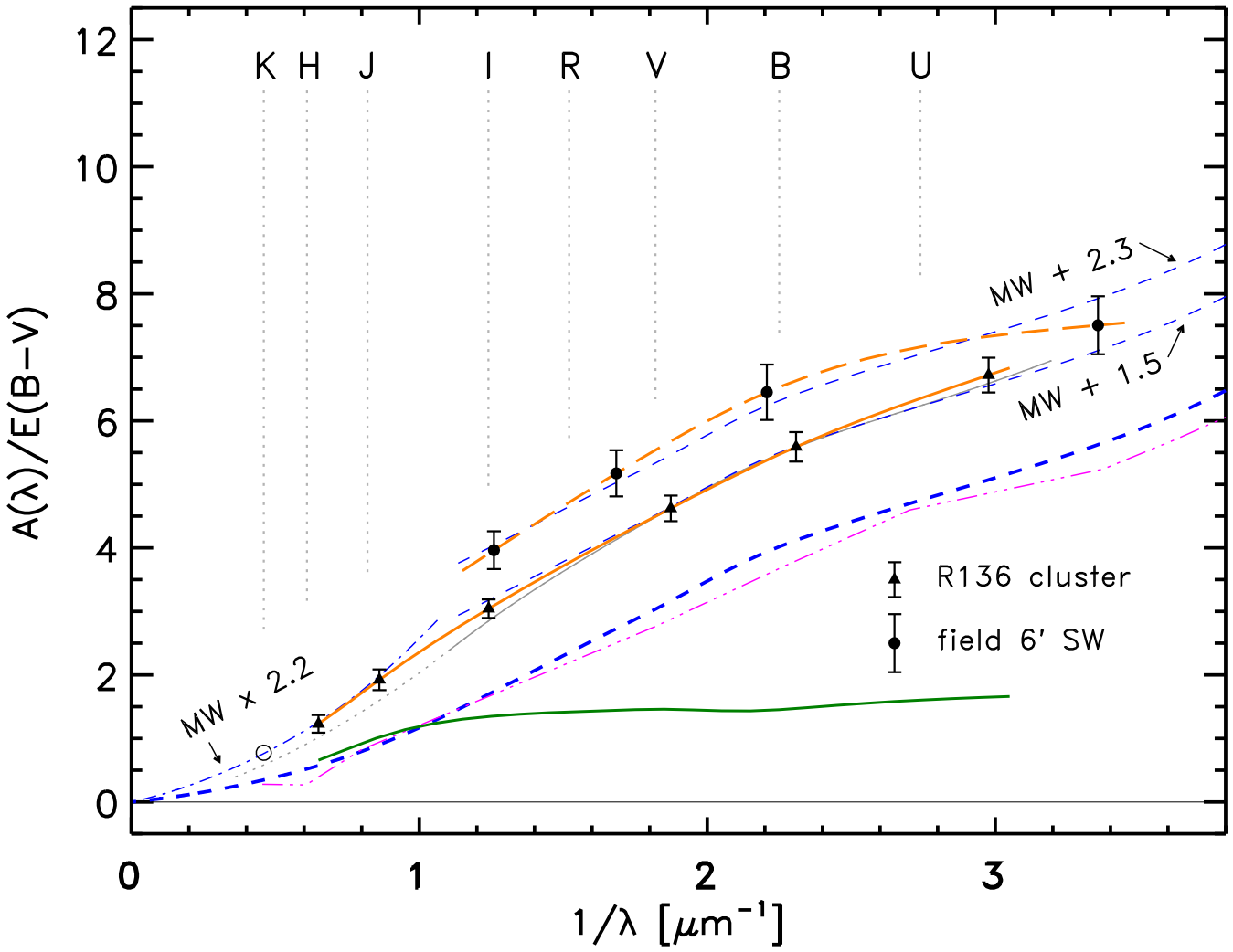

Figure 4. Extinction law. The squares and triangles show the measurements derived in the core of 30 Dor from the CMDs as a function of, respectively, $m_{438} - m_{555}$ and $m_{555} - m_{814}$ colours (the error bars for the $m_{555} - m_{814}$ data are often smaller than the symbols). The dots correspond to the measurements in the region 6′ SW of the centre studied in Paper I. The solid and long-dashed lines are a spline interpolation through those values. The short-dashed line indicates the canonical Galactic extinction law, taken from Fitzpatrick & Massa (1999) for $R_V = 3.1$. The thin dashed lines show the same law, shortwards of $\sim 1\,\mu$m shifted vertically by 1.5 and 2.3. The dot-dashed line is the Galactic extinction law, longwards $\sim 1\,\mu$m, multiplied by 2.2 to fit the measured values in the J and H bands. The green solid line is the difference between the Galactic extinction law (thick dashed line) and that of the R 136 cluster (orange solid line). The thin solid line, extended by a dotted line longwards of 9 000Å, is the extinction law of Maíz Apellániz et al. (2014) for $R_V = 4.4$. The thin triple-dot-dashed line is the extinction curve of Gordon et al. (2003) for a field around 30 Dor.

in Figure 4 and at optical wavelengths it approaches the Galactic extinction law (short dashed line). Hence, although this extinction curve cannot be considered representative of 30 Dor, it provides a good reference for the surrounding regions. The significant difference between our measurements and the extinction curve of Gordon et al. (2003), and at NIR wavelength also that of Maíz Apellániz et al. (2014), is also visible in Figure 5. A subset of the curves of Figure 4 are shown here in units of $E(\lambda - V)/E(B - V) \equiv (A_\lambda - A_V)/E(B - V) \equiv R_\lambda - R_V$, in such a way that they are all normalised in the V band. It is important to understand that this type of graph only shows the *relative* differences between the curves, but Figure 4 reveals that there are also important differences in the absolute value of the extinction, hence in the value of R_V.

For the 83 OB stars in their sample, Maíz Apellániz et al. (2014) obtain an apparently wide spread of R_V values, namely 4.4 ± 0.7, although the 50 stars with the smallest uncertainty on R_V (0.2 or less) indicate a smaller spread, namely ± 0.4. The thin solid line in Figure 4 corresponds to $R_V = 4.4$ and provides a good fit to our optical data.

The very good agreement between the R_V values measured by us and by Maíz Apellániz et al. (2014) is noteworthy, because they are derived from stars of different types, namely RGs in our case and OB stars in theirs. In principle, when the extinction is obtained from B and V photometry alone, the colour excess $E(B - V)$ corresponding to a given value of A_V, and hence the derived value of R_V, will depend on the intrinsic colour of the stars used for the measurements. McCall (2004) has extensively discussed and quantified this effect, showing that the R_V value obtained from giants with $(B - V)_0 \simeq 1$ like our RC stars could be about $\sim 10\,\%$ larger than that estimated from hot stars with $(B - V)_0 \simeq 0$. This happens because the effective wavelengths of both bands become redder, but more in B than in V and hence the extinction in B is reduced more than in V. In this way $E(B - V)$ is lowered with respect to A_V and R_V appears higher. However, the importance of these effects

Table 4. Interpolated values of R_λ for the most common bands. The table also gives the effective wavelengths (λ) and wave numbers ($1/\lambda$) of the filters, the value of R_λ^{MW} for the canonical extinction law in the diffuse Galactic ISM, and the difference between the latter and our measurements. All values are given for the specific monochromatic effective wavelength as indicated, without considering the width of the filters. Values in the K band are indicated in italics as they are extrapolated.

Band	λ [Å]	$1/\lambda$ [μm^{-1}]	R_λ	R_λ^{MW}	$R_\lambda - R_\lambda^{MW}$
U	3 650	2.74	6.35 ± 0.23	4.75	1.60
B	4 450	2.25	5.48 ± 0.20	4.02	1.46
V	5 510	1.82	4.48 ± 0.17	3.02	1.46
R	6 580	1.52	3.77 ± 0.15	2.35	1.42
I	8 060	1.24	3.04 ± 0.13	1.67	1.34
J	12 200	0.82	1.78 ± 0.14	0.83	0.95
H	16 300	0.61	1.12 ± 0.12	0.53	0.59
K	21 900	0.46	*0.78 ± 0.09*	0.34	*0.42*

is much lower if the $V - I$ colour is used instead. As discussed in Section 4, our extinction law R_λ is primarily based on those bands, owing to the smaller photometric uncertainties in $m_{555} - m_{814}$ (see also Table 3). Indeed, the excellent agreement between our R_V value and that obtained from spectrophotometry by Maíz Apellániz et al. (2014) confirms that there are no systematic differences in the optical domain.

Interestingly, longwards of ∼ 9 000 Å a systematic deviation between our curve and that of Maíz Apellániz et al.'s (2014) is observed. A similar deviation is seen if we compare our extinction law with that of Fitzpatrick & Massa (1990) and Cardelli et al. (1989), which is the functional form that Maíz Apellániz et al. (2014) have assumed in the NIR. However, they warn the reader that in the NIR range alternatives to the Cardelli's law cannot be excluded, given the small values of the NIR extinction of the stars in the sample. For that reason, in Figure 4 the curve of Maíz Apellániz et al. (2014) in shown with a dotted line in this spectral range. We believe that the considerable complexity of the extinction phenomenon (many different materials, many different sizes, etc.) makes it excessively hard and perhaps even futile to define a simple parametric curve to describe the observations accurately. Therefore, instead of attempting a parametric fit to the extinction curve that we have measured, we concentrate on the implications of its shape for the physical properties of the grains.

4.2 Extinction and properties of the grains

With $R_V = 4.5 \pm 0.2$, the extinction law that we measure around R 136 is considerably flatter (i.e. less steep in logarithmic terms) than the extinction law of the Galactic ISM shown by the short dashed line. The same is true for the extinction law in the field 6′ SW, where $R_V = 5.6 \pm 0.3$ (Paper I). In linear terms, the extinction law in these regions is actually almost exactly parallel to the Galactic curve, as the thin dashed lines show. The latter are simply the portion of the Galactic law shortwards of 1 μm shifted vertically by an offset of 1.5 and 2.3, respectively, and provide a surprisingly good fit to our observations inside R 136 and in the neighbouring field. Note that also the optical portion of the extinction curve of Gordon et al. (2003) is parallel to our measurements, and if shifted vertically by an offset of 1.6 and 2.4, respectively, it provides a good fit to our observations.

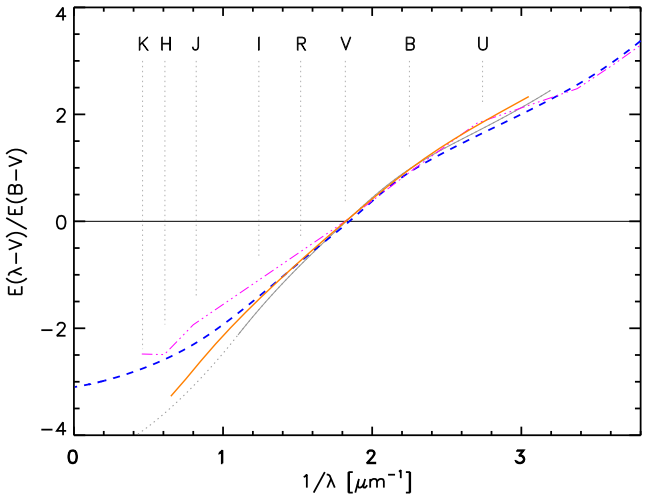

Figure 5. A subset of the extinction curves from Figure 4 is shown here, with the same line types, in units of the colour excess, i.e. $E(\lambda-V)/E(B-V)$. This figure can make it easier to compare our results with previous works. Even when all curves are renormalized in the V band, as in this figure, a marked difference remains at $\lambda > 7\,000$ Å between our measurements and the extinction curve of Gordon et al. (2003; triple-dot-dashed line) longwards of the R band.

The green solid line shown in Figure 4 represents the difference between the extinction law in R 136 and that in the Galaxy, that we take as a template. The difference is indeed remarkably flat shortwards of ∼ 1 μm (see also Table 4). This very fact indicates that the extinction law in 30 Dor is of a type similar to that of the MW (and of the regions around the Tarantula nebula), but that there is an additional component, whose contribution is "grey" in the optical, where it does not depend on wavelength. This means that there must be a larger fraction of large grains, compared to that of the diffuse Galactic ISM and the surroundings of 30 Dor.

At wavelengths longwards of 1 μm, the extinction law in 30 Dor falls off as $\sim \lambda^{-1.5}$, virtually indistinguishable from the observed behaviour of the MW extinction law (Cardelli et al. 1989), thereby indicating that the nature of the grains is the same. Indeed, the dot-dashed line shown in Figure 4 is simply the portion of the Galactic extinction law longwards of 1 μm multiplied by a factor of 2.2. We see that it fits the observations in the J and H bands quite well.

A detailed modeling of the extinction curve is beyond the scope of this work and will be deferred to a future paper. However, there are simple considerations that can provide valuable insights into the properties of the additional dust component that is present in the 30 Dor nebula.

It is well known (*e.g.,* van de Hulst 1957; Greenberg 1968; Draine & Lee 1984) that at wavelengths short enough the extinction cross section of a grain tends asymptotically to its geometric cross section $\sigma_{\rm geom} = \pi a^2$, where a denotes the grain radius. At longer wavelengths the extinction is essentially pure absorption and the cross section is smaller than $\sigma_{\rm geom}$, being proportional to $\sigma_{\rm geom} \times 2\pi a/\lambda$. Conveniently enough, the transition occurs approximately at $\lambda_0 \sim 2\pi a$. Thus, for a fixed grain size, one would expect a sort of a step function behaviour with the transition occurring abruptly around λ_0.

On the other hand, the Galactic extinction law is seen to increase steadily with the wave number λ^{-1}, over a wide range of wavelengths, say, from $\lambda \sim 5\,\mu$m or $\lambda^{-1} = 0.2\,\mu m^{-1}$ to $\lambda \sim 0.1\,\mu$m

or $\lambda^{-1} = 10\,\mu\mathrm{m}^{-1}$. This is the reason why to account for the MW extinction law a grain size distribution as been invoked, with an approximate form of a power-law $f(a) \propto a^{-3.5}$ within the interval from $a_{\rm max} \sim 0.2\,\mu$m and $a_{\rm min} \sim 0.01\,\mu$m (Mathis, Rumpl & Nordsieck 1977; Draine & Lee 1984). With such a law one can reproduce the observations quite well, essentially as a sum of step functions in which the large grain extinction dominates at the longer wavelengths and progressively smaller grains account for the increasing extinction at shorter wavelengths.

It is worth noting that, for a size distribution $f(a) \propto a^{-\beta}$ with $\beta < 4$, at wavelengths longer than $2\,\pi\,a_{\rm max}$ the extinction is dominated by the largest grains and is proportional to the total mass in grains. As shown in Figure 4, the 30 Dor nebula extinction law can be represented by the sum of a standard MW extinction curve plus one produced by an additional component of large grains (solid brown curve). The fact that in the NIR the total extinction towards R 136 is about twice as high as in the MW implies that the total mass in large grains is about twice as high as in the MW. This conclusion should be regarded in relative terms, in the sense that the relative abundance of the large grains must be a factor of 2.2 higher.

Large R values are typical of dense, still relatively quiescent clouds, that have not yet undergone extensive star formation. An example is the Orion nebula, where $R_V \simeq 5$ (e.g. Johnson 1967; Lee 1968). Like in 30 Dor, the dust in Orion is dense-cloud dust that is now being exposed to hot young stars and its extinction curve is dominated by large grains (e.g. Cardelli & Clayton 1988). A higher relative abundance of large grains may be obtained in at least three different ways: *i)* selective destruction of small grains so as to skew the size distribution in favour of large grains; *ii)* selective condensation of material on the surface of small grains, making them effectively bigger; *iii)* selective injection of "fresh" large grains into the MW mix.

The first option may be discounted because it would imply an UV extinction law that is flatter than that in the MW, whereas in fact a steep rise in the UV has been measured towards stars of the Magellanic Clouds, as compared to MW objects (*e.g.* Fitzpatrick 1998). The second option would create the same problem as the first one and, in addition, it would require an efficient condensation process to operate on the surfaces of the grains.

The third scenario looks more likely, because adding new large grains could easily account for the presence of the new component of the extinction curve, without conflicting against any existing evidence at other wavelengths, most notably the UV. Furthermore, injection of large grains is an exciting possibility opened by recent *Herschel* and *ALMA* observations of SN 1987A (Matsuura et al. 2011; Indebetouw et al. 2014). These observations suggest that a substantial amount ($> 0.4\,\mathrm{M}_\odot$) of large grains ($> 0.1\,\mu$m) were created in the ejecta of the supernova. That large grains are indeed formed in SNe has been recently established for SN 2010jl (Gall et al. 2014). Thus if one assumes that a comparable output follows *all* Type II supernova explosions, it would be easy to understand why regions of recent star formation may display the presence of a higher content of large grains. Within this scenario, one would expect that in regions where star formation was active in the recent past, say, ~ 50 Myr (i.e. the lifetime of $8\,\mathrm{M}_\odot$ stars that represent the lower mass limit of supernova type II progenitors), the excess of large grains should be highest. Such an excess would be definitely higher than in the diffuse ISM, and should be possibly higher than that in regions of ongoing star formation (age $\lesssim 5 - 10$ Myr) because the enrichment of large grains has not started yet or has not lasted long enough to produce noticeable effects.

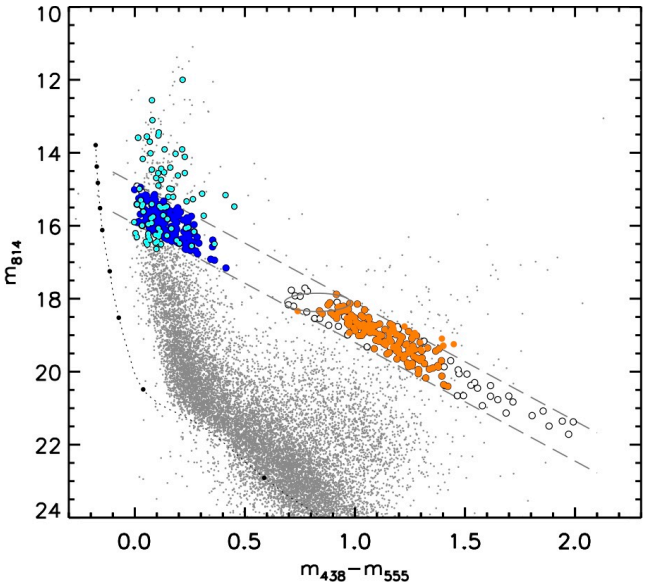

Figure 6. CMD showing selected UMS and RC stars for the study of the properties of the absorbing material. All objects indicated as thick dots have $\delta_3 < 0.1$. Those marked in blue and orange have even more accurate photometry in all optical bands ($\delta_4 < 0.1$). The stars indicated in cyan are those in the sample of Maíz Apellániz et al. (2014). The dashed lines are tangent to the spread ellipse around the nominal RC location (also shown) and parallel to the reddening vector. The ZAMS of Marigo et al. (2008) for $Z = 0.007$ is shown by the dotted line and already includes the foreground Galactic extinction. The points corresponding to masses of 1, 2, 5, 9, 15, 20, 30, 40, and 60 $\mathrm{M}_\odot$ are indicated.

UV observations of early-type stars in this region reaching down to wavelengths of $\sim 1\,200 - 1\,500$ Å are needed to probe the distribution of small grains and understand whether the additional component that we have detected is only composed of large grains or whether smaller grains are also present and in which proportion. These observations are possible with the *Cosmic Origin Spectrograph* on board the HST.

5 REDDENING DISTRIBUTION

Since we have derived the extinction law characteristic of this region, we can measure the extinction towards any object in the field whose nominal location in the CMD is known. This is the case of the RC stars and of those in the upper MS (UMS).

Zaritsky (1999) used observations from the Magellanic Clouds Photometric Survey (Harris, Zaritsky & Thompson 1997) to study the reddening distribution towards hot ($T_{\rm eff} > 12\,000$ K) and cold ($5\,500\,\mathrm{K} < T_{\rm eff} < 6\,500$ K) stars, finding that the former appear on average more extinguished than the latter. However, in Paper I we showed that this is not always the case: in the field that we studied, located about 6′ SW of 30 Dor, UMS stars span a narrower range of $E(B-V)$ values than RC objects. A similar conclusion has been reached by Sabbi et al. (2013) in their preliminary study of the Tarantula nebula. In the following we explore the distribution of the absorbing material in the core of 30 Dor, using the information contained in the optical colour–colour (CC) and colour–magnitude diagrams. We do not consider NIR bands here because our NIR photometry covers a substantially smaller field and because the lower NIR extinction can be measured in fewer stars.

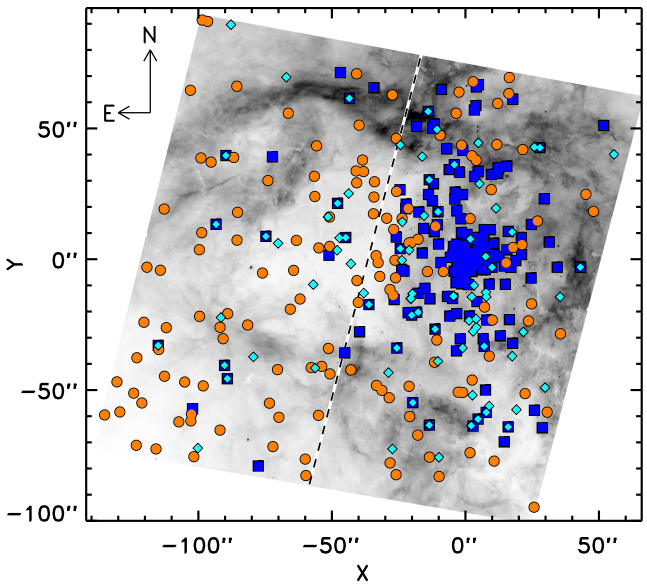

Figure 7. Location of the selected UMS and RC stars across the field. The objects in orange and blue are, respectively, the RC and UMS stars shown in Figure 6. The objects in cyan are the 83 O-type and B-type stars studied spectroscopically by Maíz Apellániz et al. (2014). The dashed line divides the region in two parts, the eastern and western half-fields, each containing half (70) of the bona-fide RC stars.

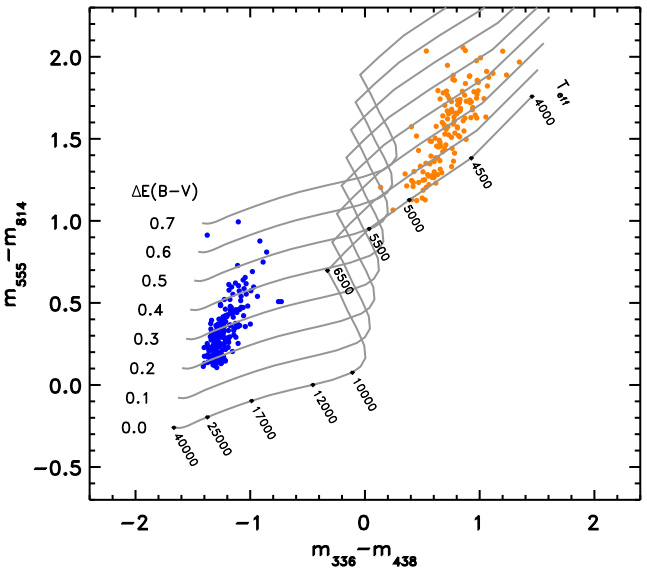

Figure 8. Colour–colour diagrams of the UMS and RC stars shown in blue and orange, respectively, in Figure 6 and 7. The solid curves provide the theoretical colours from the models of Bessell et al. (1998) for stars with gravity $\log g = 4.5$, metallicity $Z = 0.007$ and effective temperature in the range 4 000 K – 40 000 K, as indicated. All curves already include the foreground MW extinction towards the LMC and each of them corresponds to a different level of attenuation, indicated by the $\Delta E(B-V)$ value.

The objects that we have used for this study are indicated as thick symbols in the m_{814} *vs.* $m_{438} - m_{555}$ CMD of Figure 6. They include the 140 bona-fide RC stars (shown in orange) and an additional 202 UMS stars (blue) selected along the extension of the reddening vector defined by the RC. The dashed lines in the figure are tangent to the spread ellipse around the nominal RC location (also shown) and parallel to the reddening vector. Like in the case of the RC stars, the UMS objects were selected to have a combined photometric uncertainty in all optical bands of 0.1 mag or less (i.e., $\delta_4 < 0.1$) and $W_{\rm eq}(H\alpha) < 3$ Å. The objects marked in cyan in the figure are the 83 stars studied spectroscopically by Maíz Apellániz et al. (2014) that we will later compare to our UMS stars. All blue objects in our and Maíz Apellániz et al.'s sample have measured colours $B-V \geq 0$. The spatial location of all these objects is shown in Figure 7.

In Section 5.1 we will discuss the reddening distribution towards this sample of UMS and RC stars using the CC diagram. Furthermore, in Section 5.2 we will add to this sample the objects marked as thick circles in Figure 6 (45 stars in total). These RC stars are typically fainter than the rest (most have $I \gtrsim 20$), and their photometric uncertainty in the U band is somewhat larger, typically ~ 0.2 mag. Therefore, these objects do not meet the condition $\delta_4 < 0.1$ that we have imposed to select the bona-fide RC stars discussed in Section 3. However, their combined photometric uncertainty in the B, V and I bands still fully meets that condition, i.e. with $\delta_3 < 0.1$ these objects have excellent photometry in these bands. Their inclusion in the sample will prove crucial to study more extinguished RC stars that are otherwise not easily detectable in our shallower U-band exposures.

5.1 Reddening from the colour–colour plane

We begin by studying the reddening distribution in the CC diagram of Figure 8, obtained by combining all available optical bands. For now, we consider only stars with $\delta_4 < 0.1$, namely the 140 bona-fide RC stars and the 202 UMS objects shown in Figure 6, respectively, in blue and orange (the colours of the symbols stay the same). The "S"-shaped solid curve at the bottom of Figure 8 (marked 0.0) corresponds to the theoretical colours from the models of Bessell, Castelli & Plez (1998) for stars with gravity $\log g = 4.5$, metallicity $Z = 0.007$ and effective temperature in the range 4 000 K – 40 000 K, for the specific WFC 3 bands used here (the values of the effective temperature are indicated along the curve). The curve already includes the foreground MW contribution to the reddening, i.e. $E(B-V) = 0.07$.

The S-curve moves in the CC plane according to the attenuation caused by the extinction in each band. As we discussed in Paper I, although R_λ is fixed by the extinction law at a specific wavelength, for a given $E(B-V)$ the observed extinction value A_λ depends on the spectrum of the star, because it is integrated over the entire filter bandwidth. This effect is more pronounced for cold stars than for hot stars and for blue filters than for red filters (see Romaniello et al. 2002; Girardi et al. 2008). To produce the other S-curves of Figure 8, with $\Delta E(B-V) > 0$, we have applied to the models of Bessell et al. (1998) mentioned above an attenuation corresponding to incremental values of $E(B-V)$, assuming the extinction specific to this region as derived in the previous section. We have calculated the attenuation over the entire wavelength range covered by the models, for values of $\Delta E(B-V)$ ranging from 0 to 1 in steps of 0.01 mag. Using *Synphot* (Laidler et al. 2005), we have folded the attenuated models through the specific WFC 3 bands and derived the corresponding magnitudes in the HST system. The various S-curves in Figure 8 correspond to values of $\Delta E(B-V)$ ranging from 0 to 0.7 in steps of 0.1, as indicated.

Inspection of Figure 8 reveals that UMS stars span a narrower range of $\Delta E(B-V)$ values than RC objects, and all of them have $\Delta E(B-V) > 0.18$. This difference is also seen in Figure 9, showing separately the histograms of the distribution of RC stars (or-

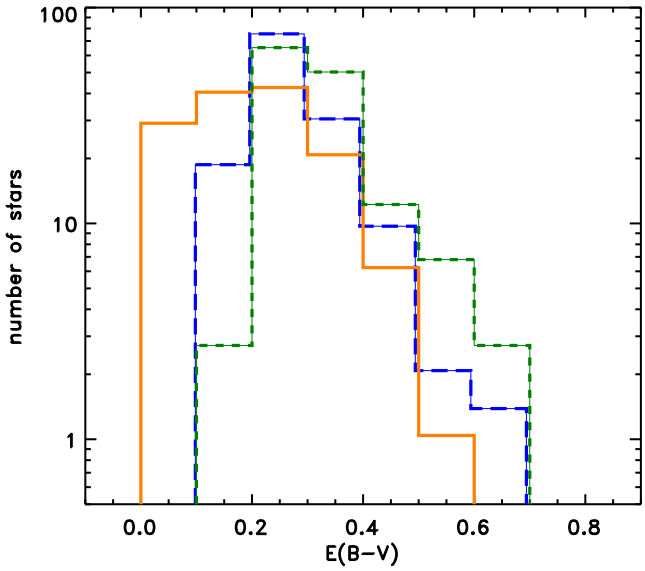

Figure 9. Histograms of the $E(B-V)$ distributions towards UMS stars (blue dashed lines) and RC stars (orange solid lines). The three panels correspond to those of Figure 8. The green short-dashed line in panel a) is the histogram of the $E(B-V)$ distribution measured by Maíz Apellániz et al. (2014) in this field.

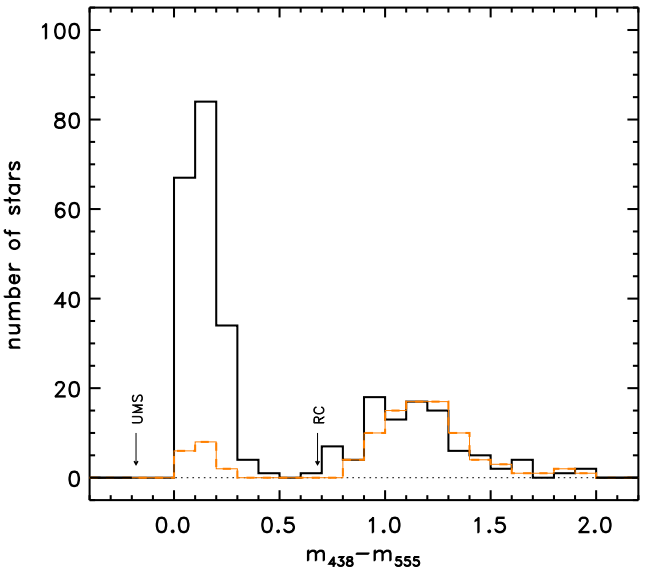

Figure 10. Histograms of the observed $m_{438} - m_{555}$ colours of the UMS and RC stars contained inside the dashed lines in Figure 6. The solid line corresponds to the stars in the western half-field and the dashed line to those in the eastern half-field. The arrows indicate the bluest expected colours of an UMS or RC stars, taking into account the $E(B-V) = 0.07$ intervening Galactic extinction.

ange solid line) and UMS stars (blue long-dashed line), with the latter rescaled to the same number of stars as RC objects. A smaller spread of $E(B-V)$ for UMS stars is not surprising, because the UMS stars are associated with R 136 and have a limited spatial distribution along the line of sight.

The $\Delta E(B-V)$ values that we have derived for the UMS stars can be compared with with those derived spectroscopically in the same field by Maíz Apellániz et al. (2014). These authors have analysed a total of 67 O-type stars and 16 B-type stars, for which spectra are available in the range $\sim 4\,000 - 5\,000$ Å at a spectral resolution $R \simeq 8\,000$ from the "VLT–FLAMES Tarantula Survey" (Evans et al. 2011). These stars are indicated as cyan dots in Figures 6 and 7. Having determined the spectral types for these objects allows Maíz Apellániz et al. (2014) to derive an accurate value of the extinction towards each of them. The green short-dashed line in Figure 9 shows the histogram of their $E(B-V)$ distribution. For ease of comparison with our results, we have shifted the histogram of Maíz Apellániz et al. (2014) by 0.07 mag to the left, to account for the foreground MW extinction, since that is not included in our $\Delta E(B-V)$ values. The reddening distribution is very similar to the one we found. The only statistically significant difference is in the number of stars with $\Delta E(B-V) = 0.15$ and we attribute this to the different composition of the two samples, since ours is exclusively made up of late O-type stars in the range $20 - 40\,M_\odot$, while the objects in Maíz Apellániz et al.'s (2014) study range from early O-type stars to early B-type objects (see Figure 6).

From this comparison we conclude that the $E(B-V)$ values that we derive are reliable, also for UMS stars, confirming that for young massive stars our method is a solid and relatively simple way to study the amount and properties of the extinction from photometry alone, with no need for spectroscopy. Provided that there are enough RC stars in the field and the level of extinction is high and variable, our method allows us to derive a robust extinction law and the absolute value of the extinction towards most UMS and RC stars.

5.2 Reddening from the colour–magnitude plane

The histograms in Figure 9 also appear to indicate that, within the uncertainties, the maximum extinction value is substantially the same for UMS and RC stars. However, we already know that some of the most extinguished RC objects are missing in our U-band photometry because it is shallower than in the other bands, thereby limiting the spread in the measured distribution. As discussed in Section 3, after an initial selection of candidates in each CMD, we retained as bona-fide RC stars only those classified as such in all CMDs simultaneously. This is a necessary step to ensure that the derived extinction law is robust and accurate at all wavelengths, but it implies that the band with shallowest exposures (U in our case) limits the most extinguished and hence faintest RC stars that we can retain in our sample. On the other hand, since we have already derived the extinction law, for the study of the reddening distribution we can rely on the CMDs based on the deepest exposures.

To this end, we have used the I *vs.* $B-V$ CMD of Figure 6, since in these bands the exposures are deeper and still sample a relatively wide spectral range ($\sim 4\,000 - 9\,000$ Å). We have selected all the objects inside the strip shown in Figure 6, parallel to the reddening vector in this plane, with combined photometric uncertainty in the three bands $\delta_3 < 0.1$. As before, we have excluded from the sample all stars with $W_{\rm eq}(H\alpha) > 3$ Å. There are a total of 381 objects satisfying these conditions: the 202 UMS stars discussed above and 179 objects that have $B-V > 0.7$ and are likely to be RC stars. Most of them are the bona-fide RC objects discussed above, to which we have added the 45 stars indicated as thick circles in Figure 6.

The histograms shown in Figure 10 provide the distribution of the observed $m_{438} - m_{555}$ colours of these 381 stars.[2] The solid line

[2] Although the m_{438} and m_{555} bands do not exactly coincide with the Johnson B and V bands, the difference is not significant in the context of the discussion that follows and we will ignore it.

corresponds to the stars in the western half-field, where R 136 is located, while the dashed line is for the objects in the eastern half-field. The arrows indicate the bluest expected colours of an UMS or RC stars after the $E(B-V) = 0.07$ intervening MW extinction is taken into account.

Figure 10 confirms that in all cases the $\Delta E(B-V)$ spread, calculated from the vertical arrows, is larger for RC stars than for UMS stars, as we already concluded from Figure 9. In addition, here there are systematically more highly extinguished RC stars, which were not detected in the shallower U band exposures and thus did not appear in Figure 9. Zaritsky (1999) had concluded that, on average, in the LMC young stars are more obscured by dust than old stars, but this conclusion too was based on a sample of stars detected simultaneously in the U, B, V, and I bands. As mentioned above and as already pointed out by Sabbi et al. (2013), this selection criterion penalizes the most extinguished evolved stars, thereby resulting in an incomplete reddening statistics.

The presence of more extinguished RC stars than UMS objects has important implications for the distribution of the absorbing material. In particular, the UMS stars in our field are associated with R 136: they have a limited spatial distribution along the line of sight and their main source of extinction is the molecular cloud from which R 136 formed. The presence of more extinguished RC stars indicates that the absorbing material is present along the line of sight also well behind R 136. Also in the eastern half-field (orange dashed line) are the RC stars more heavily reddened than UMS objects, but an important difference with respect to the western half-field is that here the minimum $\Delta E(B-V)$ value towards RC stars is ~ 0.2 larger. This implies that there is an additional extinction component in front of the eastern half-field, roughly coinciding with the silhouette of a "Christmas tree" in Figure 1.

The most straightforward explanation is that the absorbing material in the Christmas tree area is an outflow associated with a previous star formation episode in that area, some $\sim$ 50 Myr ago. The outflow has been driven outward, towards the observer, by winds and supernova explosions from former massive stars through an opening in the confining molecular cloud. Indeed, the region of the Christmas tree coincides with a blue-shifted outflow with a velocity of 100 km s^{-1} (Chu & Kennicutt 1994), as one would expect from stellar winds and supernova explosions.The average density of the material and the associated column density are lower than in the original star forming region, as confirmed by the low emission at IR (e.g. Indebetouw et al. 2009) and radio wavelengths (e.g. Johansson et al. 1998; Rubio et al. 1998). The outflow extends in our direction and causes an appreciable extinction in the foreground.

Velocities in excess of 10 km s^{-1} are typical of the outflows powered by massive stars in Orion (*e.g.,* Bally 2007), thus in 50 Myr or so this absorbing component has had time to extend few hundred parsec towards the observer and now affects also RC stars in the foreground of 30 Dor. Conversely, RC stars in the foreground of R 136, in the western half-field, are not affected by this material and the extinction towards them is lower. Previous HST observations (De Marchi et al. 2011b) have revealed a conspicuous population of $\sim$ 30 Myr old PMS stars in the eastern half-field, indicating that star formation was indeed ongoing in this area well before the birth of the R 136 cluster. It is the $> 8\,M_\odot$ stars belonging to that generation that were responsible for the injection of larger grains in the ISM when they exploded as supernovae.

The absence of objects with $E(B-V) < 0.2$ inside the Christmas-tree region is evident in Figure 11, showing the spatial distribution of the RC stars across the entire field with progressively darker shades of grey. Although there are 37 RC stars inside the area outlined by the dotted line, or 21 % of the total, none of them have $E(B-V) < 0.2$. In this region also stars with $E(B-V) > 0.6$ are missing, indicating that the total column density is lower than elsewhere in the field, in excellent agreement with the evacuated region revealed by the X ray observations of Townsley et al. (2006) in this area. In general, Figure 11 provides a map of the column density towards all RC stars and, if the spatial density of these objects is known or is assumed to be uniform, it can be used to constrain the distribution of the absorbing material along the line of sight. This will be the topic of a forthcoming paper (Panagia & De Marchi, in preparation).

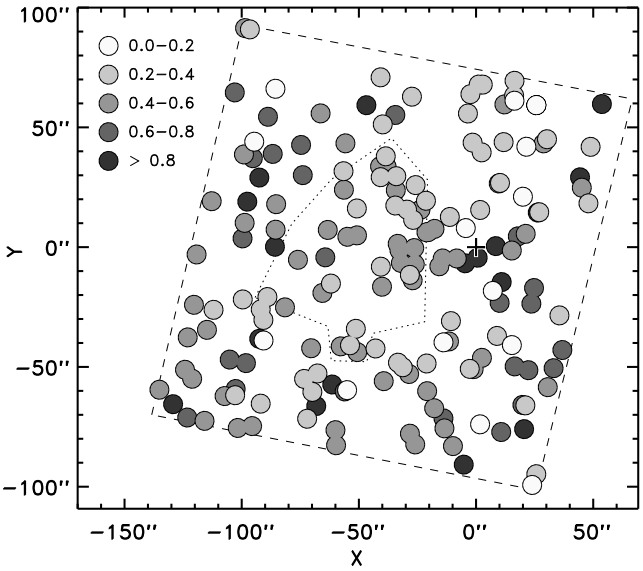

Figure 11. Distribution of the RC stars across the entire field. Progressively darker shades of grey correspond to progressively higher $E(B-V)$ values, as per the legend. The area of the Christmas tree contains no stars with $E(B-V) < 0.2$.

6 SUMMARY AND CONCLUSIONS

Using WFC 3 observations of the core of 30 Dor (De Marchi et al. 2011a), we have studied the properties of interstellar extinction in the U, B, V, I, J, and H bands over a field of 2.′7 × 2.′7 including the central R 136 cluster. We have taken advantage of the considerable and uneven levels of extinction in this field, which affect the colours and magnitudes of RC stars and spread them across the CMD. Following the method developed in Paper I, we have derived in an accurate and quantitative way both the extinction law R_λ in the wavelength range $\sim 0.3 - 1.6\,\mu$m and the values of the absolute extinction A_λ/A_V towards $\sim$ 180 RC objects as well as $\sim$ 200 O-type stars. The main results of this work can be summarised as follows.

(i) Comparing our observations in all bands with the theoretical colours and magnitudes of RC stars, we define the region of the CMDs where reddening can place RC stars. In this region we find a total of 146 objects detected in all optical bands and with a combined photometric uncertainty $\delta_4 < 0.1$ mag, 93 of which are also detected in the NIR bands covering a smaller area. We exclude from this sample 6 stars (of which 3 in the NIR) that have $W_{\rm eq}(H\alpha) > 3$ Å as they could be contaminating PMS stars. The resulting sample of

bona-fide RC stars includes 140 objects, of which 90 also covered by the NIR observations.

(ii) We derive the best linear fit to the distribution of the bona-fide RC stars in all CMDs, obtaining in this way the absolute extinction and the ratio R between absolute and selective extinction in the specific WFC 3 bands. Interpolation at the wavelengths of the Johnson B and V bands provides the extinction curve in the canonical form $R_\lambda \equiv A_\lambda/E(B-V)$, in the range $\sim 0.3 - 1.6\,\mu$m.

(iii) With $R_V = 4.5 \pm 0.2$, the extinction law that we measure in R 136 is considerably flatter than that of the diffuse Galactic ISM ($R_V = 3.1$). Furthermore, while the laws by Cardelli et al. (1989), Fitzpatrick & Massa (1990), and Maíz Apellániz et al. (2014) may provide a good fit to our extinction curve at optical wavelengths with R_V suitably close to 4.5, none of them offers a good fit to the NIR observations. Instead, the extinction curve of R 136 is best represented at optical wavelengths by the Galactic curve shifted vertically by an offset of 1.5. Longwards of 1 μm the extinction is very well matched by the Galactic law multiplied by a factor of 2.2. This implies that in R 136 the relative fraction of large grains is a factor of 2.2 higher.

(iv) We interpret the observed extinction curve as the result of an excess component of large grains added to the canonical grain distribution typical of the diffuse Galactic ISM. This is consistent with the selective injection by Type II supernova explosions of "fresh" large grains into a MW mix, as recently revealed by *Herschel* and *ALMA* observations of SN 1987A.

(v) Having derived the extinction curve in R 136, we study the relative distribution of stars and dust in the field by comparing the extinction towards individual RC and UMS stars. The $E(B-V)$ values measured towards 179 uniformly distributed RC stars provide a map of the column density in the region. The map is richly populated, since in the typical Magellanic Clouds HST field we can count on a surface density of 20 such stars per arcmin^2. We also study the extinction towards 202 UMS stars and find that they span a narrower range of $E(B-V)$ values than RC stars. The same result was found in Paper I in a field located 6′ SW of the cluster. This is at odds with the conclusions of Zaritsky (1999), who found that in the LMC stars with $T_{\rm eff} < 12\,000$ K are typically affected by larger extinction than stars with $T_{\rm eff} = 5\,500 - 6\,500$ K. We conclude that the apparent absence of heavily reddened evolved stars in Zaritsky's (1999) sample was caused by a selection effect, namely by his exclusion of hard to detect stars from the U-band photometry.

(vi) We compare the $E(B-V)$ values obtained with our method with those derived spectroscopically by Maíz Apellániz et al. (2014) for a sample of 83 early type stars in the field. We find an excellent agreement, confirming the validity of our extinction determination not only for RC stars but also for O-type and B-type stars that are still on the MS.

In summary, in this work we have shown that when the levels of extinction are high and uneven, like in the case of the 30 Dor region, RC stars can be used to derive the extinction law and the absolute extinction towards those stars with an accuracy comparable with that allowed by spectroscopy of early-type stars. Furthermore, since RC stars sample in a uniform way a much larger volume than early-type stars, they can provide a characterisation of the extinction and a measure of the column density also outside the most active star forming regions and over multiple lines of sight.

We have also shown that in the range $\sim 0.3 - 1.6\,\mu$m the extinction curve of R 136 is not satisfactorily described by the widely used single-parameter families of extinction laws (e.g. Cardelli et al. 1989; Fitzpatrick & Massa 1990). This is not unexpected, since Gordon et al. (2003) had already shown that the the extinction curve in the LMC2 Supershell around 30 Dor and along most lines of sight in the LMC do not follow the Cardelli et al. (1989) relationship based on R_V. In principle, it is practical to have a parametric description, but the extinction law is governed by the interplay of scattering and absorption due to grains with different physical properties, including chemical composition and size, and located in different environments. Therefore, one wonders whether it is possible and meaningful to look for a mathematical formulation able to capture the complexity revealed by the observations, particularly when one needs to cover a wide spectral range.

Instead, it is very important to study the properties of the extinction curve in light of the current and recent star formation history experienced by the regions. So far our investigation using this method has covered two fields in the LMC, one containing R 136 and one located 6′ SW of it. We are going to extend the study to the entire Tarantula nebula, which was recently observed as part of the Hubble Tarantula Treasury Program (Sabbi et al. 2013). These observations sample a large contiguous area on the sky (168 arcmin^2) in the range $\sim 0.25 - 1.6\,\mu$m and will allow us to also explore how smaller grains contribute to the extinction in regions with different intensity of the current and most recent star formation.

ACKNOWLEDGMENTS

We are grateful to our referee, Prof. Geoff Clayton, for insightful comments that have helped us to improve the presentation of this work. This paper is based on Early Release Science observations made by the WFC 3 Scientific Oversight Committee. NP acknowledges partial support by STScI–DDRF grant D0001.82435.

REFERENCES

Bally J., 2007, Ap&SS, 311, 15
Bessell M., Castelli F., Plez B., 1998, A&A, 333, 231
Bless R., Savage B., 1972, ApJ, 171, 293
Cardelli J., Clayton G., 1988, AJ, 95, 516
Cardelli J., Clayton G., Mathis J., 1988, ApJ, 329, L33
Cardelli J., Clayton G., Mathis J., 1989, ApJ, 345, 245
Cardelli J., Sembach K., Mathis J., 1992, AJ, 104, 1916
Chu Y.-H., Kennicutt R., 1994, ApJ, 425, 720
Clayton G., Martin P., 1985, ApJ, 288, 558
De Marchi G., et al., 2011a, ApJ, 739, 27
De Marchi G., et al., 2011b, ApJ, 740, 11
De Marchi G., Panagia N., Girardi L., 2014, MNRAS, 438, 513
De Marchi G., Panagia N., Romaniello M., 2010, ApJ, 715, 1
De Marchi G., Panagia N., Sabbi E., 2011, ApJ, 740, 10
Draine B., Lee H., 1984, ApJ, 285, 89
Evans C., et al., 2011, A&A, 530, A108
Fitzpatrick E., 1998, in Ultraviolet Astrophysics Beyond the IUE Final Archive, ed. W. Wamsteker, R. Gonzalez Riestra (Noordwijk: ESA), 461
Fitzpatrick E., 1999, PASP, 111, 63
Fitzpatrick E., Massa D., 1990, ApJS, 72, 163
Fitzpatrick E., Massa D., 1999, ApJ, 525, 1011
Fitzpatrick E., Massa D., 2005, AJ, 130, 1127
Fitzpatrick E., Massa D., 2007, ApJ, 663, 320
Fitzpatrick E., Savage B., 1984, ApJ, 279, 578
Gall C., et al., 2014, Nature, 511, 326
Geha M., et al., 1998, AJ, 115, 1045
Girardi L., et al., 2008, PASP, 120, 583
Gordon K., Clayton G., Misselt K., Landolt A., Wolff M., 2003, ApJ, 594, 279

Gottlieb D., Upson W., 1969, ApJ, 157, 611
Greenberg J. M., 1968, in Nebulae and interstellar matter, ed. B. Middlehurst, L. Aller (Chicago: Univ. Chicago Press), 221
Harris J., Zaritsky D., Thompson I., 1997, AJ, 114, 1933
Haschke R., Grebel E., Duffau S., 2011, AJ, 141, 158
Heckman T., et al., 2004, ApJ, 613, 109
Hill V., Andrievsky S., Spite M., 1995, A&A, 293, 347
Hunter D., et al., 1995, ApJ, 444, 758
Indebetouw R., et al., 2009, ApJ, 694, 84
Indebetouw R., et al., 2014, ApJ, 782, L2
Johansson L., et al. 1998, A&A, 331, 857
Johnson H., 1967, ApJ, 150, L39
Johnson H., Mendoza E., 1964, Boletin de los Obs. de Tonantzintla y Tacubaya, 3, 311
Johnson H., 1968, in Nebulae and interstellar matter, ed. B. Middlehurst, L. Aller (Chicago: Univ. Chicago Press), 167
Laidler V., et al, 2005, Synphot User's Guide, (Baltimore: STScI)
Lebouteiller V., Bernard-Salas J., Brandl B., et al., 2008, ApJ, 680, 398
Lee T., 1968, ApJ, 152, 913
Lilly S., Le Fevre O., Hammer F., Crampton D., 1996, ApJ, 460, L1
Madau P., et al., 1996, MNRAS, 283, 1388
Maíz Apellániz J., 2004, PASP, 116, 859
Maíz Apellániz J., et al., 2014, A&A, 564, A63
Marigo P., et al., 2008, A&A, 482, 883
Massa D., Savage B., Fitzpatrick E., 1983, ApJ, 266, 662
Mathis J., Rumpl W., Nordsieck K., 1977, ApJ, 217, 425
Matsuura M., et al., 2011, Sci, 333, 1258
McCall M., 2004, AJ, 128, 2144
Meurer G., Heckman T., Lehnert M., Leitherer C., Lowenthal J., 1997, AJ, 114, 54
Misselt K., Clayton G., Gordon K., 1999, ApJ, 512, 128
Panagia N., 1999, in New Views of the Magellanic Clouds, ed. Y.-H. Chu, N. Suntzeff, J. Hesser, D. Bohlender (San Francisco: ASP), 549
Panagia N., Gilmozzi R., Macchetto F., Adorf H.-M., Kirshner R., 1991, ApJ, 380, L23
Romaniello M., 1998, PhD thesis, Scuola Normale Superiore, Pisa, Italy
Romaniello M., Panagia N., Scuderi S., Kirshner R., 2002, AJ, 123, 915
Rubio M., et al., 1998, AJ, 116, 1708
Sabbi E., et al., 2013, AJ, 146, 53
Seaton M., 1979, MNRAS, 187, 73P
Shapley A., Steidel C., Pettini M., Adelberger K., 2003, ApJ, 588, 65
Savage B., Mathis J., 1979, ARA&A, 17, 73
Tatton B., et al., 2013, A&A, 554, A33
Townsley L., et al., 2006, AJ, 131, 2140
Valencic L., Clayton G., Gordon K., 2004, ApJ, 616, 912
van de Hulst H., 1957, Light scattering by small particles, (New York: Wiley & Sons)
Walborn N., Blades J., 1997, ApJS, 112, 457
White R., Basri G., 2003, ApJ, 582, 1109
Zaritsky D., 1999, AJ, 118, 2824